

DEVELOPMENT OF A 15 T Nb_3Sn ACCELERATOR DIPOLE DEMONSTRATOR AT FERMILAB

I. Novitski, N. Andreev, E. Barzi, J. Carmichael, V. V. Kashikhin, D. Turrioni, M. Yu, and A. V. Zlobin

Abstract— A 100 TeV scale Hadron Collider (HC) with a nominal operation field of at least 15 T is being considered for the post-LHC era, which requires using the Nb_3Sn technology. Practical demonstration of this field level in an accelerator-quality magnet and substantial reduction of the magnet costs are the key conditions for realization of such a machine. FNAL has started the development of a 15 T Nb_3Sn dipole demonstrator for a 100 TeV scale HC. The magnet design is based on 4-layer shell type coils, graded between the inner and outer layers to maximize the performance and reduce the cost. The experience gained during the Nb_3Sn magnet R&D is applied to different aspects of the magnet design. This paper describes the magnetic and structural designs and parameters of the 15 T Nb_3Sn dipole and the steps towards the demonstration model fabrication.

Index Terms— Dipole magnet, collider, magnetic field, mechanical structure, Nb_3Sn superconductor.

I. INTRODUCTION

HADRON COLLIDERS (HC) are the most powerful discovery tools in modern high energy physics. Interest in an HC with energy above the LHC reach has gained further momentum in the strategic plans recently developed in the U.S., Europe and China [1]-[3]. To build a ~ 100 TeV center of mass energy HC in a ~ 100 km tunnel, dipoles with a nominal operation field of ~ 15 T and $\sim 20\%$ margin are needed. A nominal field of ~ 15 T can be provided only by the Nb_3Sn technology. A practical demonstration of this field level in accelerator-quality magnets and a substantial reduction of magnet costs are key conditions for the realization of such a machine.

The foremost challenges for 15 T Nb_3Sn magnets include considerably larger coil volume, higher Lorentz forces and larger stored energy than in present accelerator magnets. The coil width, necessary to achieve the 15 T field level, requires 4-layer coil design [4]. The stronger forces produce higher stresses in the coil and in the magnet mechanical structure and, thus, stress control tools may be needed to keep stresses at an acceptable level for the brittle Nb_3Sn conductor. The large stored energy also leads to additional complications in the magnet quench protection.

FNAL has started the development of a 15 T Nb_3Sn dipole demonstrator for a 100 TeV scale HC based on the optimized “cos-theta” coil design [4], [5]. The experience gained at FNAL during the Nb_3Sn accelerator magnet R&D for VLHC and LHC upgrades [6], [7], will be applied to all stages of the magnet design and fabrication. The main objectives of this magnet are

demonstration of the 15 T field level in an aperture suitable for future HC and study of the magnet quench performance and margins, quench protection and field quality. This paper describes the design concept and parameters of the 15 T Nb_3Sn dipole demonstrator. Magnet cable test results, and magnetic and structural analyses are reported and discussed.

II. MAGNET DESIGN AND PARAMETERS

Five 4-layer graded coil cross-sections were designed using ROXIE code [8] based on the two cables with 15 mm width and various thicknesses listed in Table I [4]. The cables use 1.0 mm and 0.7 mm Nb_3Sn strands with a critical current density J_c of 1500 A/mm^2 at 15 T and 4.2 K, and a nominal Cu/SC ratio of 1.13. Similar Nb_3Sn cables have already been developed at FNAL and used in earlier dipole models [9], [10].

TABLE I
DIMENSIONS OF REACTED BARE CABLES.

Parameter	Units	Cable 1	Cable 2
Number of strands		28	40
Mid-thickness	mm	1.870	1.319
Width	mm	15.10	15.10
Keystone angle	degree	0.805	0.805

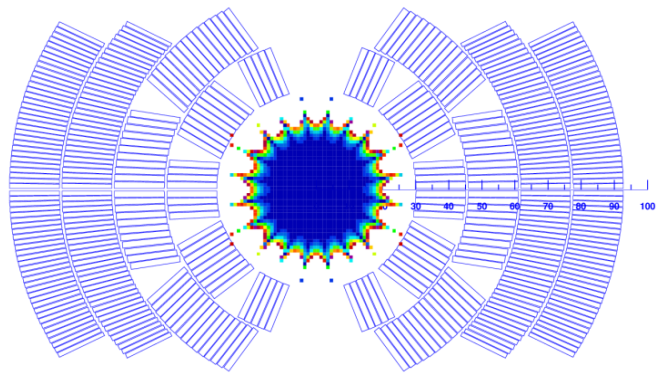


Fig. 1. Coil cross-section with field quality diagram in the coil aperture. The dark zone represents a field uniformity better than 2×10^{-4} .

Based on the design studies described in [4], a 4-layer graded coil with minimized number of turns was selected for the 15 T dipole demonstrator. The coil cross-section is shown in Fig. 1. The two innermost layers have five blocks separated by three wedges. The two outermost layers do not use wedges. The large

field harmonics generated by the two outermost layers were compensated by optimizing the number of turns, and the wedge size and position in the two innermost layers. The resulting good field quality area in the aperture is shown in Fig. 1 by the dark zone.

The mechanical structure of the 15 T dipole demonstrator has been significantly reworked with respect to the original one described in [5] to address the large stress and deformation issues revealed by ANSYS analysis. The new cold-mass structure of the 15 T dipole demonstrator is shown in Fig. 2.

The coil assembly is surrounded by a 2 mm stainless steel spacer and supported by a vertically split iron yoke and aluminum clamps. The magnet is surrounded by a thin stainless steel bolted skin which is not a key structural element in the new support structure. The clamps (called I-clamps) interleave with the iron yoke laminations in the top and bottom sectors of the iron yoke thus reducing the iron filling factor in these areas to 50%.

The axial Lorentz forces on the coil ends are intercepted by two thick end plates connected by eight tie rods running through the dedicated holes in the iron yoke. This new support structure with aluminum I-clamps is different from the original concept based on stainless steel C-clamps and a thick skin [5]. It provides a better management of stresses inside the magnet support structure, which is explained in the following section.

The magnet cold-mass is ~ 1 m long. The maximum cold mass transverse size is ~ 610 mm, which is limited by the inner diameter of the FNAL test cryostat. Quench protection heaters composed of stainless steel strips are placed between the 2nd and 3rd coil layers and on the coil outer layer.

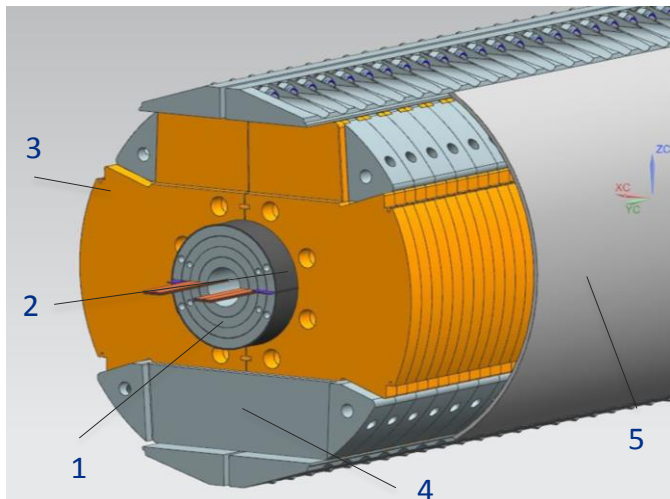


Fig. 2. Cold mass design of the 15 T dipole demonstrator: 1 – 4-layer Nb₃Sn coil; 2 – coil-yoke stainless steel spacer; 3 – iron yoke laminations; 4 – aluminum I-clamp; 5 – stainless steel bolted skin.

The calculated 2D design parameters of the 15 T dipole demonstrator are summarized in Table II. The field distribution diagrams in the coil and iron yoke are shown in Fig. 3. The maximum design bore field at 4.2 K is 15.6 T. Reducing the coil temperature to 1.9 K allows increasing the maximum bore field by $\sim 10\%$ with respect to the values shown in Table II.

TABLE II.
MAGNET DESIGN PARAMETERS AT 4.2 K

Parameter	Unit	Value
Bore field at short sample limit	T	15.61
Peak field at short sample limit	T	16.25
Current at short sample limit, I_c	kA	11.34
Inductance at I_c	mH/m	25.61
Stored energy at I_c	MJ/m	1.65
Horizontal Lorentz force per quadrant at I_c	MN/m	7.36
Vertical Lorentz force per quadrant at I_c	MN/m	-4.50

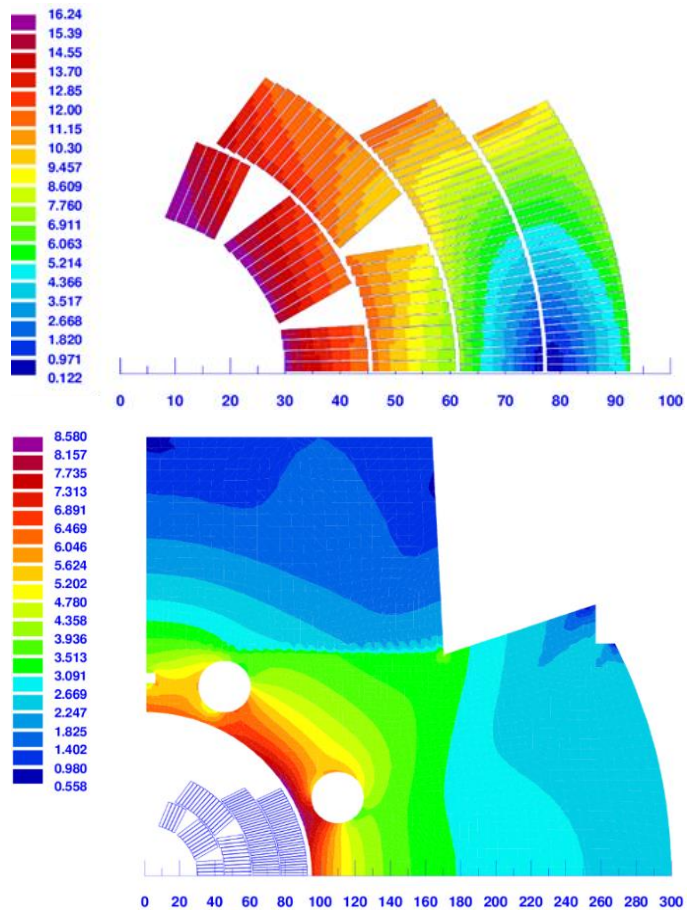


Fig. 3. 2D field distribution in the coil (top) and the iron yoke (bottom).

Calculated geometrical harmonics in the magnet straight section are summarized in Table III. Dependences of the sextupole field component as a function of field in the magnet aperture are presented in Fig. 4. All the harmonics are reported at the reference radius of 17 mm.

TABLE III.
NORMAL RELATIVE HARMONICS (10^{-4} OF THE DIPOLE COMPONENT)

Harmonic	Value
b_3	0.0018
b_5	0.0154
b_7	0.0523
b_9	0.0612

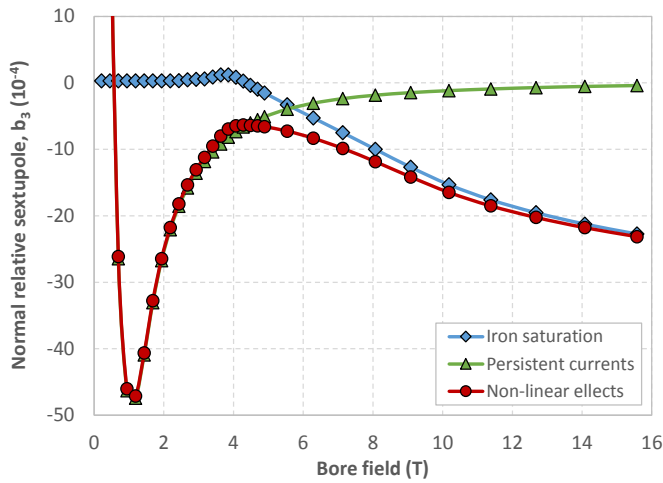


Fig. 4. Non-linear effects in the normal relative sextupole during the current ramp-up in the second excitation cycle.

There are large persistent current and iron saturation effects in the sextupole component. In the 15 T demonstrator the absolute peak value of b_3 is ~ 48 units. It is a factor of two larger than in the two-layer 11 T dipole where it reaches ~ 20 units [11] and an order of magnitude larger than in the NbTi LHC main dipoles. The variation of the normal sextupole b_3 due to the iron saturation in the 15 T dipole demonstrator is more than 20 units. No special correction is envisioned for the first dipole demonstrator since it will be used to measure the unaltered, weakly-coupled coil magnetization and iron saturation effects, and to benchmark the computation codes.

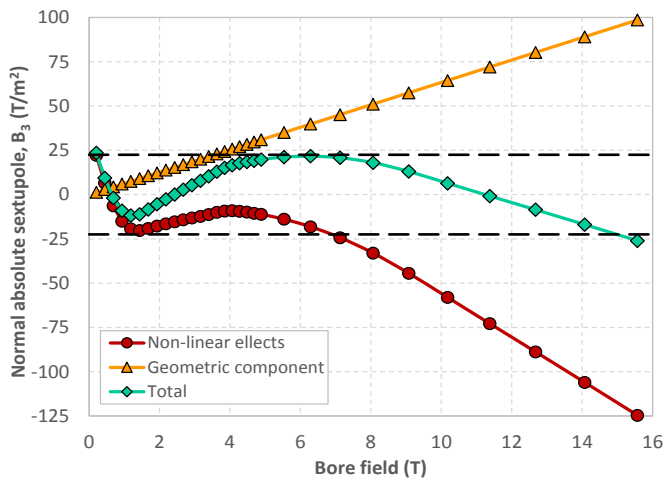


Fig. 5. Geometrical correction of non-linear effects in the normal absolute sextupole during current ramp-up in the second excitation cycle.

Since during the current ramp-up both effects have the same (negative) sign in the sextupole component, it is possible to reduce its amplitude by adding a positive geometric error, either by changing the midplane shims in the existing coils or the spacers in the new coils. An example of such a correction is shown in Fig. 5, which presents the unaltered absolute sextupole strength at the reference radius (from Fig. 4) and that after adding $+18.3$ units of the relative sextupole component into the coil geometry. The absolute value of the sextupole is used instead of the relative one to facilitate comparison with the

strength of a dedicated sextupole corrector. The horizontal dashed lines at $\pm 22.5 \text{ T/m}^2$ show the corrector strength that is necessary to compensate for the remaining sextupole perturbations in 0 to 15 T range. By applying this virtually no-cost correction technique alone, one can increase the magnet dynamic range by a factor of two for a fixed strength of sextupole corrector.

For future models, a persistent current corrector, similar to that developed for previous magnets [12] will be considered in conjunction with optimizing holes in the iron yoke. This technique was also previously used at FNAL [13] and it may help to further suppress both non-linear effects.

The 3D magnetic analysis was performed using the OPERA 3D code. Fig. 6 shows the complete 4-layer coil and the coil end design. The end length of the two outermost layers was minimized in order to increase the straight section length. Small end spacers were used in these layers to split the large blocks and reduce the accumulated turn inclination. For mechanical reasons the iron yoke is extended over the coil ends. In that case, the peak field point limiting the magnet performance is in the coil ends. To reduce the field enhancement in the coil ends with respect to the magnet straight section, the pole blocks of the two innermost layers were shifted towards the magnet center.

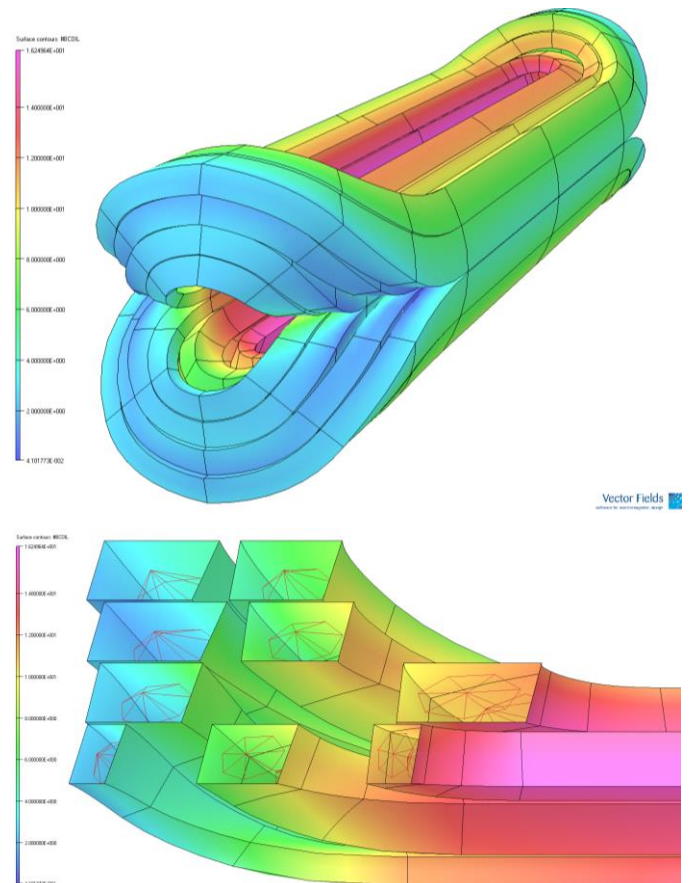


Fig. 6. Complete coil (top) and the coil end cross-section (bottom) with the magnetic flux distribution at the magnet short sample limit.

A cylindrical cut-out was also introduced in the ends of the iron yoke, as shown in Fig. 7 to reduce the peak field in the coil ends. There is a 2% field enhancement in the coil ends without the cutout. Removing $\sim 45 \text{ mm}$ of the iron yoke material around

the coil ends helps to reduce the peak field in the end to the same level of peak field in the magnet central cross-section.

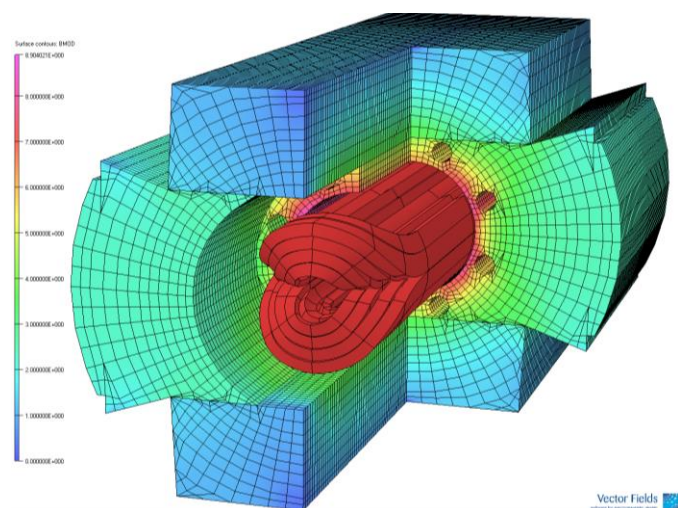


Fig. 7. 3D model with flux density in the iron yoke at the short sample limit.

The coil cross-sections, optimized with ROXIE, were input into the BEND program [14] where the three-dimensional end geometry of each group was optimized by minimizing the strain energy in the cables with respect to “bend in the hard direction”, providing also the information on turn twist and radius of curvature. Slight shifting and manual adjustments of the BEND parameters were done to produce a cable geometry that does not require bottom-supporting parts. The output files from BEND were then directly imported into a CAD package. The completed CAD geometry can then be imported into other programs for magnetic field and coupled mechanical and thermal FEA. Fig. 8 shows the coil end geometry and end parts for both the lead and return ends of the innermost coil layer. Fig. 9 shows the two outermost layers of the coil.

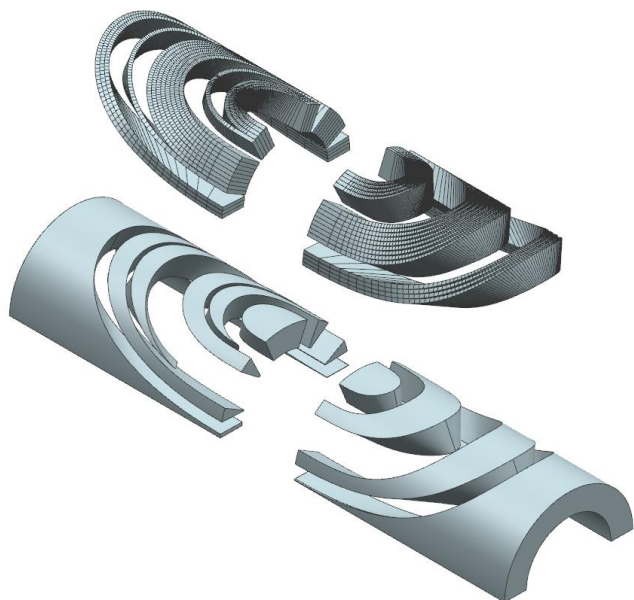


Fig. 8. The end geometry of the innermost coil layer (top) and corresponding end parts (bottom). The left and right sides of the figure correspond to the lead ends and return ends respectively.

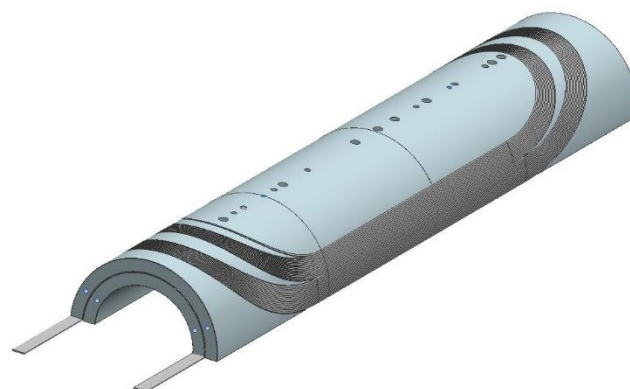


Fig. 9. The two outermost layers of the coil.

III. STRUCTURAL ANALYSIS

Finite element analysis using a parametric 2D ANSYS model has been performed to optimize the stress in the coil and major elements of the magnet support structure, and to minimize the conductor motion and magnet cross-section deformation at room and operation temperatures up to the design field of 15 T.

The ANSYS model of the 15 T dipole demonstrator in two cross-sections is shown in Fig. 10. The baseline materials used in the magnet and their properties are listed in Table IV. The data for the Nb₃Sn coil are based on measurements reported in [15]. The key criterion of the mechanical structure optimization was to maintain the coils under compression up to the design field of 15 T and the maximum coil stress below ~180 MPa during magnet assembly and operation.

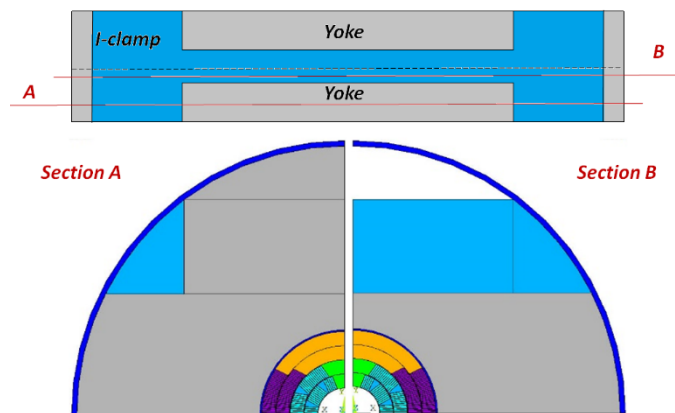


Fig. 10. ANSYS model of 15 T dipole for section A (left) and section B (right).

TABLE IV.
MATERIAL PROPERTIES

Structural element	Material	Thermal contract. (300-2 K), mm/m	Elasticity modulus, GPa		Yield stress, MPa	
			warm	cold	warm	cold
Coil (rad/azim)	Nb ₃ Sn composite	2.9/3.3	35/20	40/40	n/a	n/a
In.coil pole blocks	Ti-6Al-4V	1.7	115	125	650	>900
Out.coil pole blocks	St St	2.9	195	215	230	500
Wedges	bronze	3.2	110	120	280	350
Coil-yoke spacer	St St	2.9	190	210	230	500
Clamp	Aluminum	4.1	70	81	500	600
Yoke	Iron 1045	2.0	210	225	350	>400
Skin	St St 304L	2.9	190	210	230	500

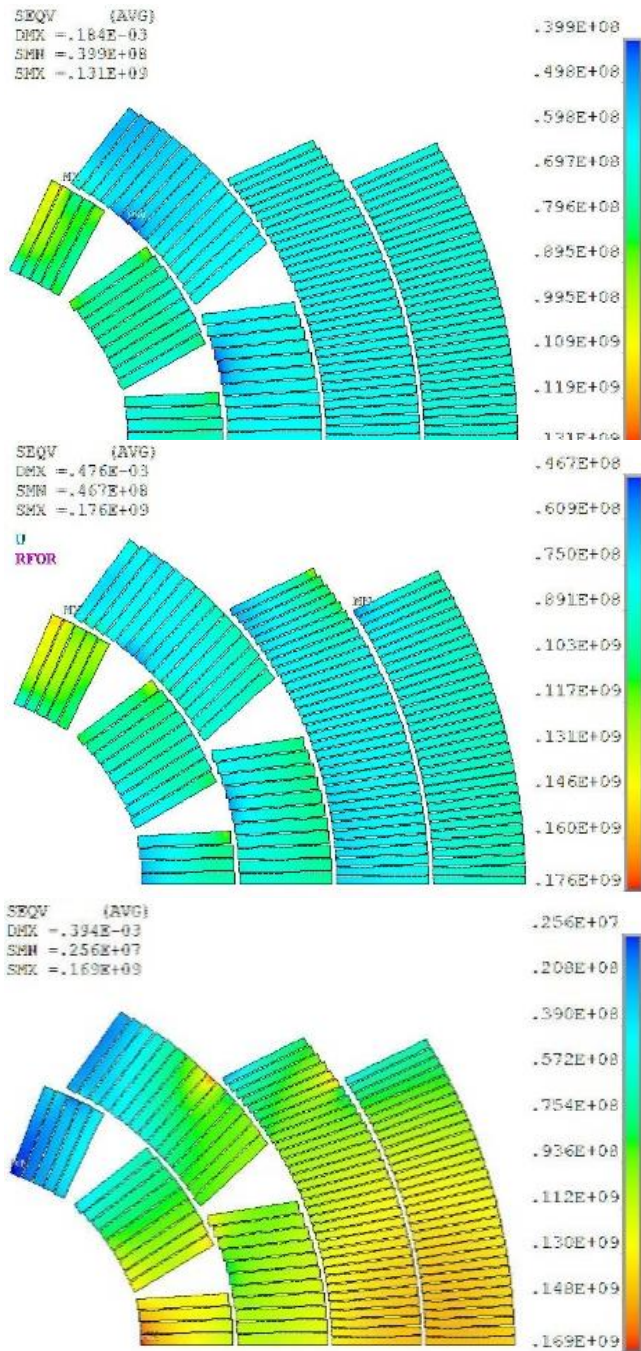


Fig. 11. Stress distribution in the coil at room temperature after assembly (top), after cooling down (middle) and at the 15 T bore field (bottom).

TABLE V.
AVERAGE AZIMUTHAL STRESS IN SELECT TURNS (MPa)

Position in coil	Azimuthal Coil Stress, MPa		
	Assembly	Cool down	B=15 T
Pole 1	92	128	3
Pole 2	62	78	15
Pole 3	74	96	27
Pole 4	75	93	53
Mid-plane 1	77	92	147
Mid-plane 2	74	107	119
Mid-plane 3	74	88	140
Mid-plane 4	78	103	145

Distribution of the equivalent stress in the coil at room temperature after assembly, after cooling down and at 15 T bore field is shown in Fig. 11. The average transverse stress in the pole and mid-plane turns of the coil layers at the above stages is summarized in Table V. The maximum equivalent coil stress at room temperature and after cooling down is in the innermost-layer pole turn is about 130 MPa and 176 MPa respectively. At the bore field of 15 T, the maximum equivalent coil stress is in the innermost layer mid-plane turns and is close to 170 MPa.

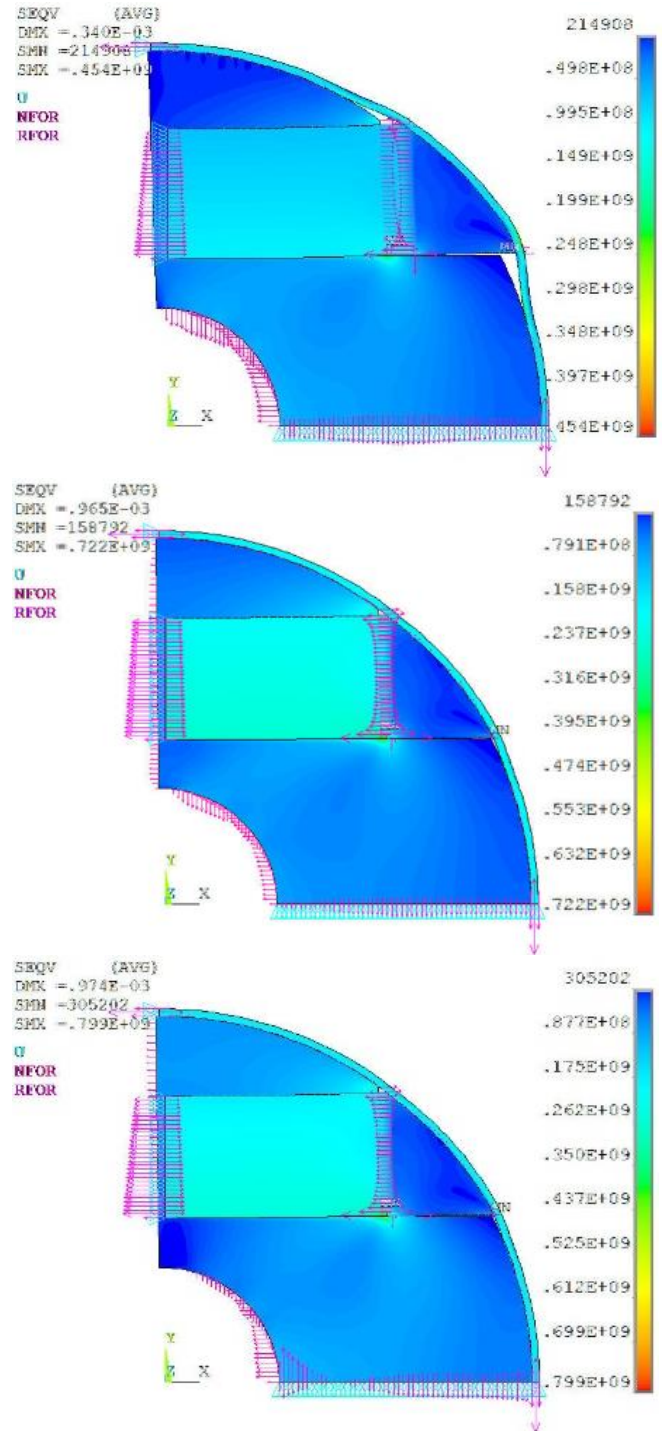


Fig. 12. Stress distribution in the support structure at room temperature after assembly (top), after cooling down (middle) and at 15 T bore field (bottom).

TABLE VI.
MAXIMUM STRESS IN STRUCTURAL ELEMENTS (MPa)

Structural element	Maximum stress, MPa		
	assembly	cool down	B=15 T
Yoke	454	722*	800*
Clamp	170	395	440
Skin	275	310	320

* number from elastic model with singularities

A stress distribution diagram in the dipole mechanical structure is shown in Fig. 12. The maximum stress values in the major elements of the magnet support structure, which were calculated at the assembly and operation stages are presented in Table VI. All results are obtained using a conservative model with elastic material properties. The stress level in clamps, iron laminations and bolted skin during magnet assembly and operation are at an acceptable level for the materials used.

IV. CABLE OPTIMIZATION

The 40-strand Rutherford cable used in the two outermost coil layers was developed and optimized for the 11 T LHC dipole [9]. No additional optimization is needed for this cable. Three unit lengths are presently available for the demonstrator dipole outer coils. A cross-section of the 40-strand Rutherford cable is shown in Fig. 13 (top).

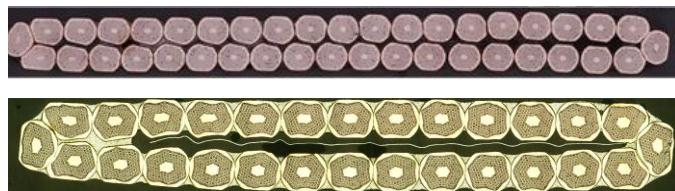


Fig. 13. Cross-sections of the 40-strand (top) and 28-strand (bottom) Rutherford cables.

The Rutherford cable with 28 strands of 1 mm diameter and 14.7 mm nominal width before reaction was developed and optimized for the 15 T dipole demonstrator using state-of-the-art RRP® wires. A cross-section of the 28-strand Rutherford cable is shown in Fig. 13 (bottom).

The cable samples were fabricated in one pass. They all included an 11 mm wide stainless steel core to suppress eddy currents and obtain better field quality and ramp rate dependence in magnets. The first series of cable samples made of RRP-108/127 strands demonstrated critical current degradation smaller than 4% over the whole packing factor range up to 92% encompassed by the cables [16]. Then cable degradation studies were continued with an RRP-150/169 wire most recently procured for the 15 T dipole demonstrator.

The critical current I_c at 4.2 K normalized to the average I_c of the virgin wire ($PF=78.5\%$) is plotted in Fig. 14 as a function of cable packing factor for two different external field values. The I_c degradation was less than 3% for cables up to ~90% cable compaction.

The Residual Resistivity Ratio (RRR) was measured as the ratio of the wire resistivity at room temperature over its residual resistivity at 19.5 K. Fig. 15 shows the RRR as a function of PF for the RRP-150/169 extracted strands. The overall RRR of the

wires decreased more or less linearly with compaction and was above 250 up to ~90% cable compaction.

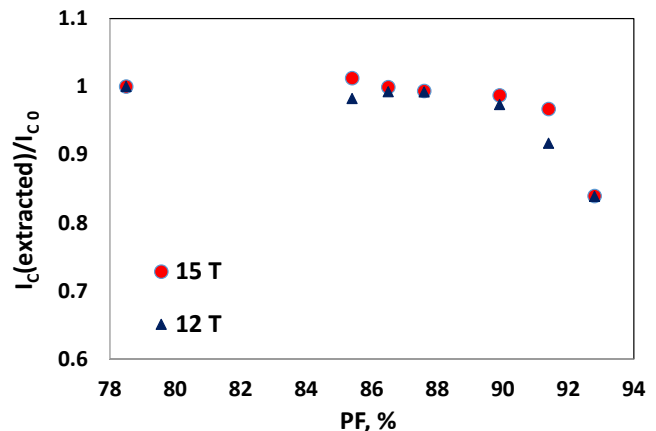


Fig. 14. Extracted strand I_c at 4.2 K normalized to I_c of virgin wire vs. cable packing factor for cables made with RRP-150/169 Nb₃Sn strands.

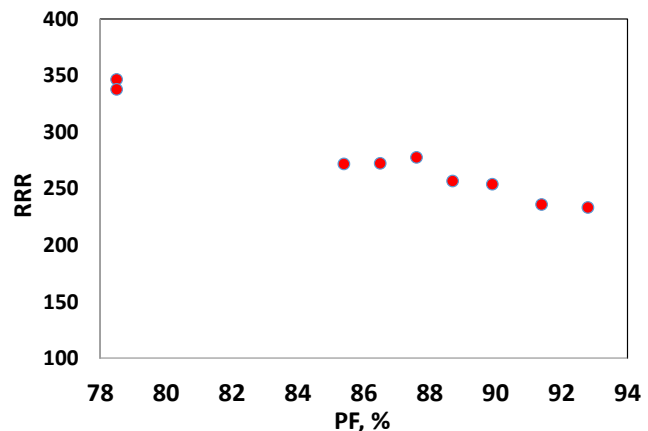


Fig. 15 RRR as a function of cable packing factor for RRP-150/169 strands.

Based on these results, the nominal cable mid-thickness that was chosen for the 15 T dipole is 1.80 mm.

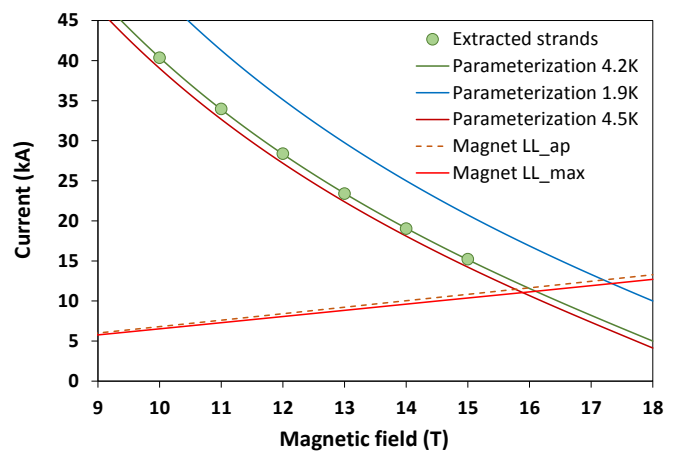


Fig. 16. Measured and parameterized $I_c(B)$ dependences for the 28-strand cable and 15 T dipole demonstrator load lines.

The $I_c(B)$ dependences, measured using extracted strands at 4.2 K, and calculated for 4.5 and 1.9 K using parameterization [17] for the 28-strand cable, are shown in Fig. 16 together with

the 15 T dipole demonstrator load lines. The magnet short sample limits estimated based on these data are 11.05 kA ($B_{ap}=15.25$ T) at 4.5 K and 12.2 kA ($B_{ap}=16.65$ T) at 1.9 K.

V. CONCLUSIONS

A 15 T Nb₃Sn dipole demonstrator for a future HC is being developed at Fermilab. Magnet design is based on a 4-layer graded block cos-theta coil with 60 mm aperture and cold iron yoke. The magnet maximum field estimated based on the cable data is 15.25 T at 4.5 K and 16.65 T at 1.9 K.

Due to the high field and large coil volume there are large non-linear iron saturation and persistent current effects in the sextupole field component. It was demonstrated that these effects can be partially compensated by a geometrical correction, which allows increasing the magnet dynamic range by more than a factor of two at virtually no cost. Further tuning of the field quality by different techniques will be explored in future models.

The magnet support structure has been optimized to manage the large level of Lorentz forces. The concept has been radically changed from the previous iteration, which revealed excessively high stresses in the magnet structure and a possible separation of the pole turns at the maximum field. It was shown that the new structure allows keeping the stresses in the coil and support structure within the acceptable limits at all conditions.

Cable samples for both inner and outer coils were fabricated and tested. Cable packing factor has been optimized to achieve a low degradation of cable critical current and copper matrix RRR. The design of a four-layer coil, including coil ends, mechanical structure and tooling is complete and being procured. Magnet fabrication and first test are planned for 2016.

ACKNOWLEDGEMENT

The authors thank the staff of FNAL Technical Division for contributions to magnet and tooling design as well as cable fabrication and test.

REFERENCES

- [1] "Building for Discovery: Strategic Plan for U.S. Particle Physics in the Global Context," P5 Report, http://science.energy.gov/~media/hep/hep/pap/pdf/May%202014/FINAL_P5_Report_053014.pdf
- [2] Future Circular Collider Study Kickoff Meeting, Geneva, Switzerland, February 12-14, 2014, <http://indico.cern.ch/event/282344/timetable/#20140212>
- [3] CEPC/SppC study in China, <http://indico.cern.ch/event/282344/session/1/contribution/65/material/slides/1.pdf>
- [4] A.V. Zlobin et al., "Design concept and parameters of a 15 T Nb₃Sn dipole demonstrator for a 100 TeV hadron collider," Proc. of IPAC2015, Richmond (VA), May 2015.
- [5] V.V. Kashikhin et al., "Magnetic and structural design of a 15 T Nb₃Sn accelerator dipole model," Proc. of CEC/ICMC2015, Tucson (AZ), 2015. *IOP Conf. Ser.: Materials Science and Engineering (MSE)*, submitted for publication.
- [6] A.V. Zlobin, "Status of Nb₃Sn Accelerator Magnet R&D at Fermilab", EuCARD - HE-LHC'10 AccNet mini-workshop on a "High-Energy LHC", 14-16 October 2010, FERMILAB-PUB-11-001-TD, CERN Yellow Report CERN-2011-003, p. 50. [arXiv:1108.1869]
- [7] A.V. Zlobin et al., "11 T Twin-Aperture Nb₃Sn Dipole Development for LHC Upgrades," *IEEE Trans. Appl. Supercond.*, v. 25, Issue 3, June 2015, 4002209.
- [8] ROXIE Code for an Electromagnetic Simulation and Optimization of Accelerator Magnets, <http://cern.ch/roxie>.
- [9] N. Andreev et al., "Development of Rutherford-type Cables for High Field Accelerator Magnets at Fermilab," *IEEE Trans. Appl. Supercond.*, v. 17, Issue 2, June 2007, p. 1027.
- [10] E. Barzi et al., "Development and Fabrication of Nb₃Sn Rutherford Cable for the 11 T DS Dipole Demonstration Model," *IEEE Trans. Appl. Supercond.*, v. 22, Issue 3, June 2012, 6000805.
- [11] B. Auchmann et al., "Magnetic Analysis of a Single-Aperture 11T Nb₃Sn Demonstrator Dipole for LHC Upgrades", Proceedings of IPAC2012, New Orleans, Louisiana, USA, p. 3596.
- [12] V.V. Kashikhin et al., "Passive Correction of the Persistent Current Effect in Nb₃Sn Accelerator Magnets," *IEEE Trans. Appl. Supercond.* vol. 13, no. 2, June 2003, p. 1270.
- [13] G. Ambrosio et al., "Magnetic Design of the Fermilab 11 T Nb₃Sn Short Dipole Model," *IEEE Trans. Appl. Supercond.* vol. 10, no. 1, March 2000, p. 322.
- [14] J. M. Cook, "Strain Energy Minimization in SSC Magnet Winding," *IEEE Trans. on Magnetics*, vol. 27, March 1991, p.1976.
- [15] D. R. Chichili et al., "Investigation of Cable Insulation and Thermo-Mechanical Properties of Epoxy Impregnated Nb₃Sn Composite," *IEEE Trans. on Applied Supercond.*, vol. 10, no. 1, 2000, p. 1317.
- [16] E. Barzi et al., "Nb₃Sn RRP® Strand and Cable Development for a 15 T Dipole Demonstrator," *this conference*.
- [17] L.T. Summers et al., "A model for the prediction of Nb₃Sn critical current as a function of field, temperature, strain and radiation damage", *IEEE Trans. on Magnetics*, 27 (2): 2041-2044 (1991).